THERMAL AND STRUCTURAL ANALYSIS OF THE EXOMARS NAVIGATION AND LOCALIZATION CAMERAS.

Christopher Pye, Pierre-Luc Messier
Maya HTT

Tim Elgin
Neptec Design Group

ABSTRACT

The European Space Agency's ExoMars rover uses a pair of identical stereo cameras for navigation and localization. The cameras must meet a demanding accuracy requirement when exposed the harsh Martian environment. This paper describes the thermal and structural analysis of the camera design. The goal was to validate the thermal performance of the camera and to determine the impact of thermo-elastic distortion on the optical performance of the camera.

The thermal analysis was performed with Simcenter 3D Space Systems Thermal and the structural analysis with NX Nastran. The paper includes the approach used to model the Mars environment and the mapping process used to transfer the temperatures from thermal to structural models.

INTRODUCTION

The ExoMars Rover, developed by ESA, provides key mission capabilities: surface mobility, subsurface drilling and automatic sample collection, processing, and distribution to instruments. It hosts a suite of analytical instruments dedicated to exobiology and geochemistry research: this is the Pasteur payload.

The Rover uses solar panels to generate the required electrical power, and is designed to survive the cold Martian nights with the help of novel batteries and heater units. Due to the infrequent communication opportunities, only 1 or 2 short sessions per sol (Martian day), the ExoMars Rover is highly autonomous. Scientists on Earth will designate target destinations on the basis of compressed stereo images acquired by the cameras mounted on the Rover mast.

The Rover must then calculate navigation solutions and safely travel approximately 100 m per sol. To achieve this, it creates digital maps from navigation stereo cameras and computes a suitable trajectory. Close-up, collision avoidance cameras, are used to ensure safety.

This paper describes the thermal and structural analysis performed on the identical navigation (top of mast) and localization (base of mast) stereo cameras.

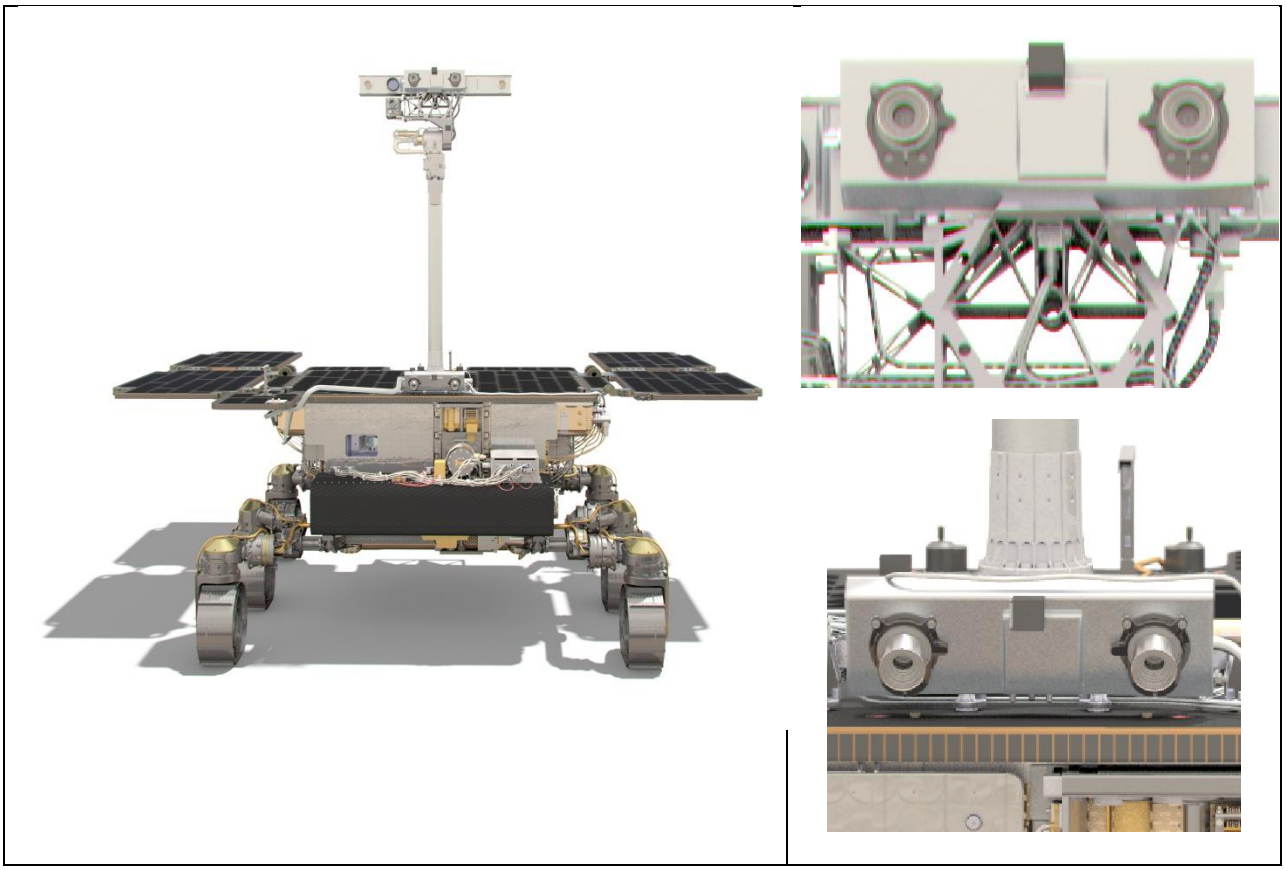

Figure 1 Artists Impression of ExoMars Rover and breakout of navigation and localization camers. Credit: ESA/ATG Medialab

THERMAL MODEL

The camera geometry was supplied as a STEP file that was imported in SC 3D and used to create the thermal and structural meshes. For the thermal analysis, the Space Systems Thermal module was used. The meshing approach for the major components is presented in Table 1.

Following meshing the total mass of the model was computed and compared with the mass computed from the CAD geometry. As expected, the model mass was less than the CAD mass. This is because small parts (fasteners, electronic components etc.) are ignored in the FE model. The model was adjusted so that each major component had the correct total mass. The some examples of mass corrections are listed in Table 2. The largest correction is for the PWB's. In the CAD model, the PWB mass includes the boards themselves, all components not explicitly modeled and the mounting hardware, in the FE model there is just the two layers of shells used to model the board. For the items in Table 2, the correction was applied by adding non-structural mass.

Table 1. Meshing Techniques

Part	Mesh Type	Comments
Front and back Housing	Shell	A separate mesh was used for the inner surface of the front and rear housing near PWB components. This provided the correct gap between component and housing for the atmospheric conduction modeling. The inner surface was non-conducting and connected to the outer surface mesh to represent through thickness conduction. All in plane-conduction was handled by the outer surface mesh.
PWBs	Shell	Separate meshes were used for each face of the PWB's. They were assigned the PWB material and half the PWB thickness. The faces were then thermally coupled to represent through thickness conduction. This is easily done by creating a Conductive Thermal Coupling, selecting each surface and specifying the thermal conductivity.
Components	Shell	Components with assigned dissipation were each modeled as a single shell element. The element was connected to the PWB with a resistance representing Resistance from junction to case and resistance from case to board in series.
Lens Glass	Solid	Tetrahedral elements. The outer glass surface was meshed with shell elements for radiation modeling. This is not necessary but simplifies selection for exterior radiation.
Lens Clamp	Solid	
Optics housings	Shell	The two (per lens) that the optical glass is mounted it were each modeled with shell elements. The thickness was set such that the modeled mass of each part was correct.

The optical components were meshed as solid elements and therefore were very close to the CAD mass. The lens enclosures have a complex shape but were modelled with a shell mesh on their exterior surfaces with a single thickness value that gives the same mass, this gives the correct mass and a reasonable approximation to the conduction, see Figure 2.

Table 2. Mass correction

Component	Initial FE Mass (gm)	CAD Mass (gm)	Final FE Mass
Rear Housing	85.1	95.8	95.8
Front Housing plus fasteners	163.0	203.0	204.5
PWB's	38.0	219.8	220.0

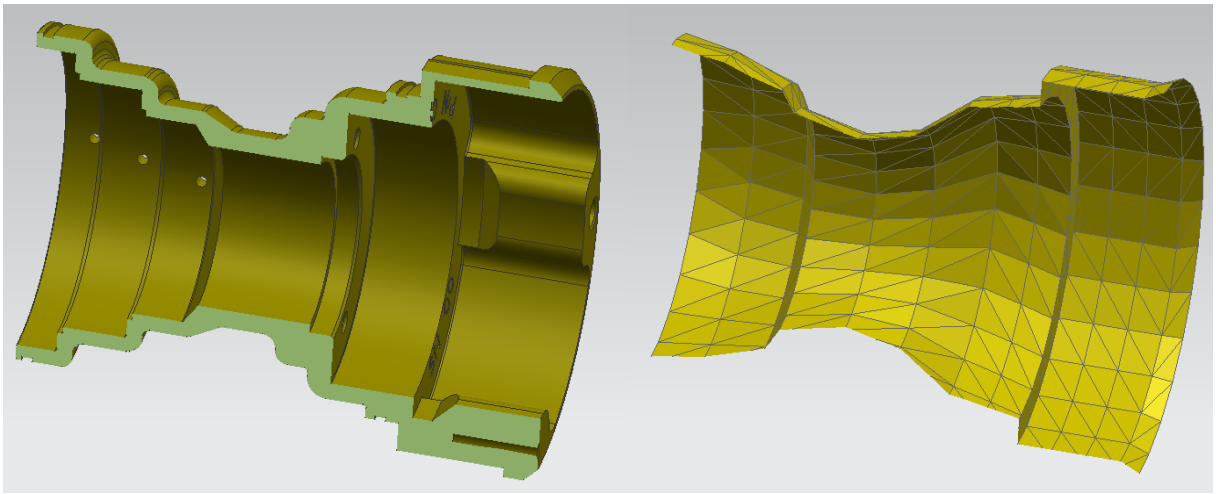

Figure 2. Lens Barrel CAD and FE representations.

MARTIAN ENVIRONMENT

The environmental conditions under which the cameras are required to operate were defined by the Rover prime contractor and passed to the camera team. Many of these values, such as ground temperature, sky temperature and fluxes were supplied as time varying values for a one sol.

The approaches used to model the various features of the Martian environment are discussed in the following sections.

Direct Solar Radiation

Direct Solar radiation was modelled using the NX SST solar heating option. The planet is selected and the latitude and model orientation defined. This also supports time varying solar fluxes and the appropriate supplied profile was used. The flux profiles include the effect of absorption by the atmosphere and so no correction for Optical Depth is included in the model. The model was placed in the Northern hemisphere and oriented with the rover facing south.

Diffuse Solar (Sky) radiation

Diffuse Solar radiation is used to model the effect of scattering of direct solar radiation due to dust in the atmosphere. NX SST supports modelling this affect but the input is based on scattering coefficients rather than optical depth. A technique was developed that used a dome of shell elements around the model that is defined as a source of diffuse solar radiation. The dome used had a radius of 30m.

This approach was validated for a simple model to show that it yields the expected heat fluxes. This approach was added as a feature of later releases of SC 3D-SST.

Sky Temperature

NX SST can automatically create an enclosure around a model to represent the space environment. This was used to represent the sky. Temperature profiles for the appropriate environment were applied to this enclosure.

Air Temperature

The elements used to model the dome were assigned the air temperature profile for each environment. The dome elements do not participate in the temperature calculations and were used as a convenient way to pass air temperature to the code used for convection calculations.

Ground Temperature

A 60m diameter disc was created to represent the Martian surface. It was assigned the Mars surface optical properties and the appropriate ground temperature profile.

Convection

Convection was modelled using Fortran code that is linked into the NX SST temperature solver. The routine has access to the required geometry information, such as element area and all model temperatures and heat loads.

The routine used the algorithm supplied to the camera team to compute a heat transfer coefficient, h, from air properties and wind speed. The heat transfer is then used to calculate the convection heat loss, Qc, from:

$$Qc = h\ A\ (T_{elem} - T_{air})$$

Where A is the area of the element, T_{elem} and T_{air} are the temperatures of the convecting element and the air, respectively. Note that this gives a positive value when the element is losing heat by convection. The computed convection heat loss is subtracted from the other heat loads calculated for the convecting element (solar radiation etc.) to represent the convection term in the model.

Heat transfer coefficients were supplied for different geometric configurations. Convecting elements were placed in one of four element groups corresponding to each configuration:

1. conv_vert for vertical surfaces
2. conv_below for horizontal surfaces with air below
3. conv_above for horizontal surfaces with air above
4. conv_cyl for horizontal cylinders

The characteristic lengths required for the convection calculations are hard coded into the convection routine with each group of elements having two characteristic lengths, one for natural convection and one for forced convection. For forced convection over flat plates the shortest side was selected for the characteristic length as it gives the highest heat transfer coefficient.

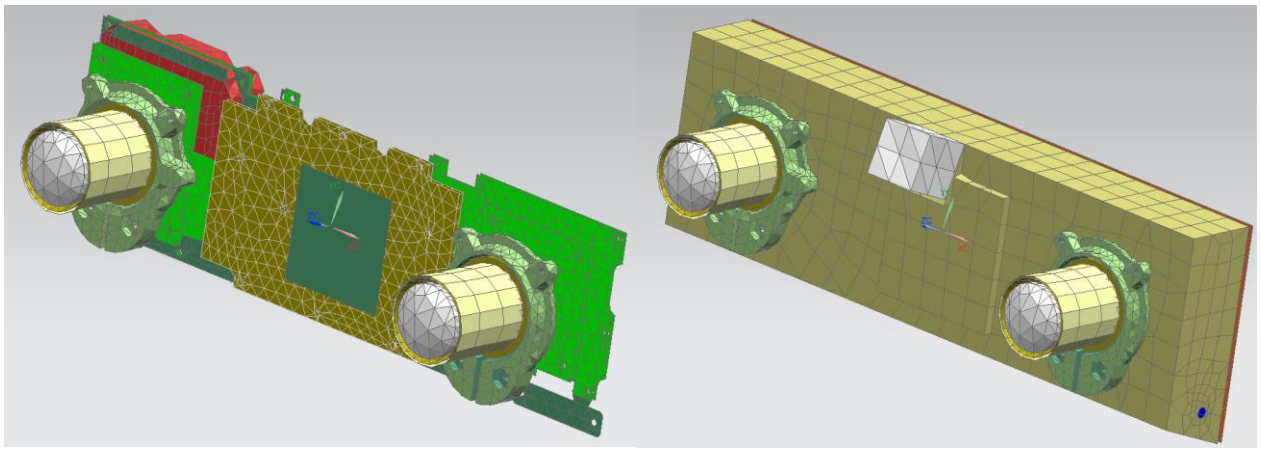

OVERALL MODEL

SC3D-SST supports the concept of Assembly FEM's. These work much the same way as part assemblies which contain instances of parts that are defined separately. The advantages of the assembly FEM approach are:

1. Each part or subassembly can be modeled independently and the model can be tested to ensure validity before being added to the Assembly FEM. The model would typically include the mesh, thermal couplings, heat loads and internal radiation.
2. If there are multiple instances of the same assembly then the same model can be instanced multiple times.
3. The task of creating the thermal model can be distributed amongst the thermal team. Each team member can focus on one component or sub-assembly then create and test a thermal model.
4. Changes to a part FEM is applied to all instances used in the Assembly FEM.

The assembly FEM approach was used to create the full thermal model. This included:

1. Martian Surface.
2. Simple model of the ExoMars rover based on supplied simplified geometry.
3. Navigation Camera.
4. Localization Camera.

The use of the assembly FEM means that any updates to the single camera model would be applied to both instances. However, the architecture used also allows the boundary conditions and heat loads applied to each instances to be independently changed, if required, to accommodate different operational scenarios for each camera.

Temperature profiles were supplied for each major rover surface, therefore the rover model could be relatively coarse.

The parts of the thermal model are generally meshed independently and then connected with thermal couplings. The methodologies used are listed in Table 3.

Table 3. Methodologies for Thermal Couplings

Physical Phenomenon	Methodology
Air gap conduction	Applied internally. Surface geometry is accurately defined and a conductive gap coupling used. The thermal conductivity set to a temperature dependent relationship appropriate for the Martian atmosphere.
Bolted joints	Total conductance per joint calculated as (number of bolts x conductance per bolt). Values taken from handbooks.
Semiconductor mounting	Use supplied θ_{jc}, θ_{jb}.
Adhesive joint or thermal filler.	Calculate equivalent heat transfer coefficient and apply.

THERMAL SOLUTION CASES

The thermal load cases used represented 25 different combinations of the following:

- Environment – seven environments were defined by parameters such as season, latitude, optical depth, atmospheric pressure and wind speed.

- Power dissipations – three power dissipation cases were defined, minimum, typical, and maximum. With total power of the typical case defined as 100% the other two cases were 93% and 136%. Component power dissipations did not all change by the same percentage. Note that power dissipation is zero at night because the camera is off and no local keep alive power is present.
- Presence of absence of dust – the presence of dust was modeled as changes in surface optical properties and transmissibility of the atmosphere. The values used were validated experimentally.

The thermal solver provides the option to run the radiation calculations and the temperature solution in parallel, either locally or using multiple machines . This was used when a single case was run. When running multiple cases greater efficiency is achieved by running each case on a single core and running the cases simultaneously.

RESULTS

One of the key points on the camera is the Temperature Reference Point (TRP), which is used by the vehicle for determining when the cameras may be safely powered on (or should they need to be, turned off during nominal operation). The TRP is located on the camera housing and is the primary temperature monitored during operation on Mars. The cameras are attached to the rover with three fasteners each with no isolation provided. The results of the analysis confirmed that the temperatures of the cameras are primarily driven by the temperature of the mounting point.

The hottest case was Environment 1 with no dust. The temperature distribution for the navigational camera, at the hottest time of day, is shown in Figure 3. The hottest component is the DC-DC converter. The primary cooling for this component is provided by ‘air’ conduction from the top of the component to the rear housing of the camera. The air gap is nominally 0.3mm. Given this small clearance, the effect of larger air gaps was investigated. Steady state runs performed on a model of just the camera showed that doubling the gap increases the DC-DC converter temperature by 10ºC. If the Martian atmosphere is removed completely, the temperature increases by 45ºC.

The coldest case temperature profiles for key components are shown in Figure 4.

Given the significance of the camera mounting point temperature on the camera’s thermal performance, the model was run with the mounting point conductance reduced to half of the nominal value. Table 4 shows the change in maximum and minimum temperatures after making this change. The most significant changes are for the NavCam hot case with the maximum temperatures increasing by almost 7 ºC and the coldest temperatures decreasing by almost 5 ºC.

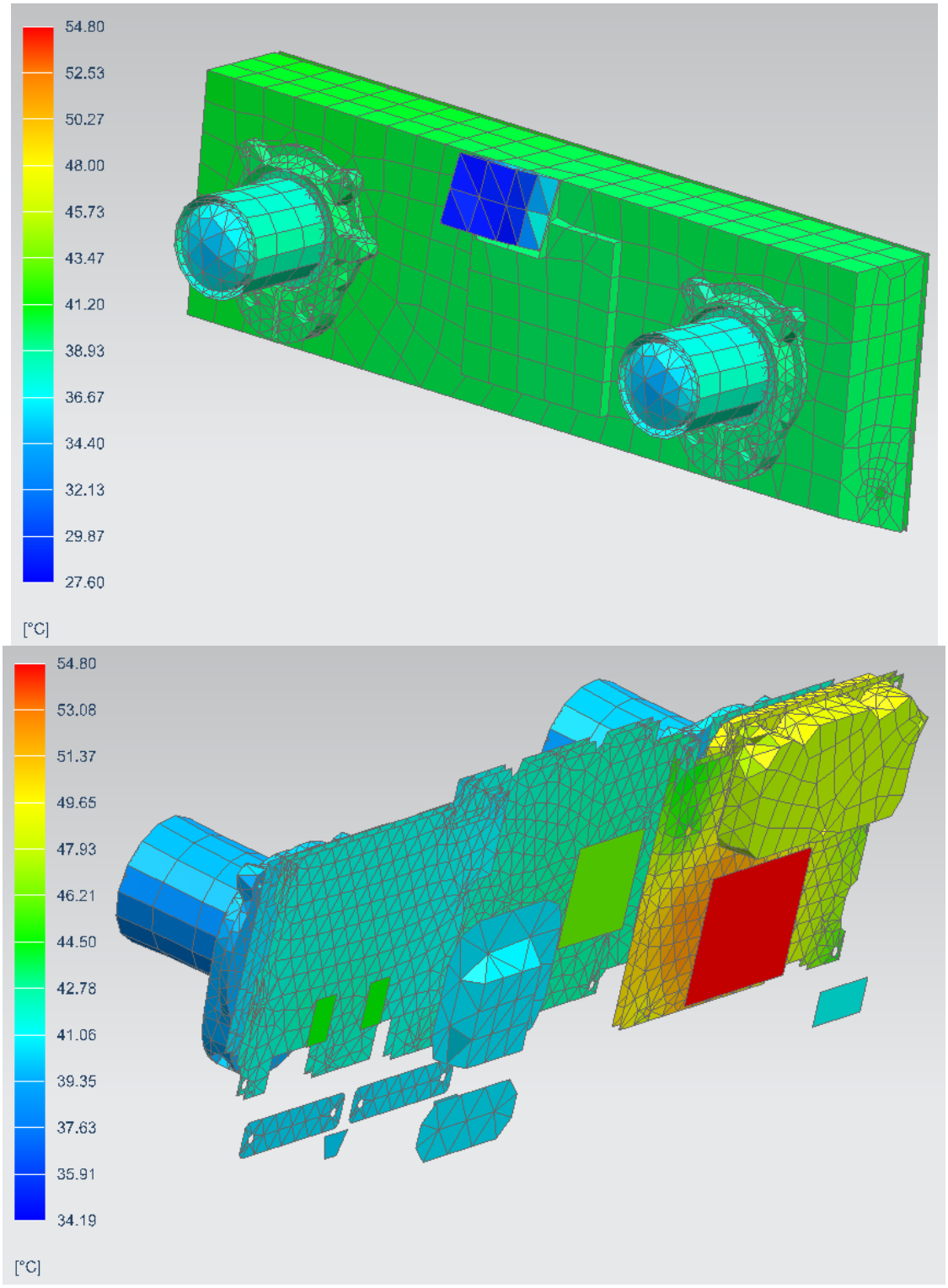

Figure 3. NavCam, Environment 1, No Dust, Hottest Temperatures

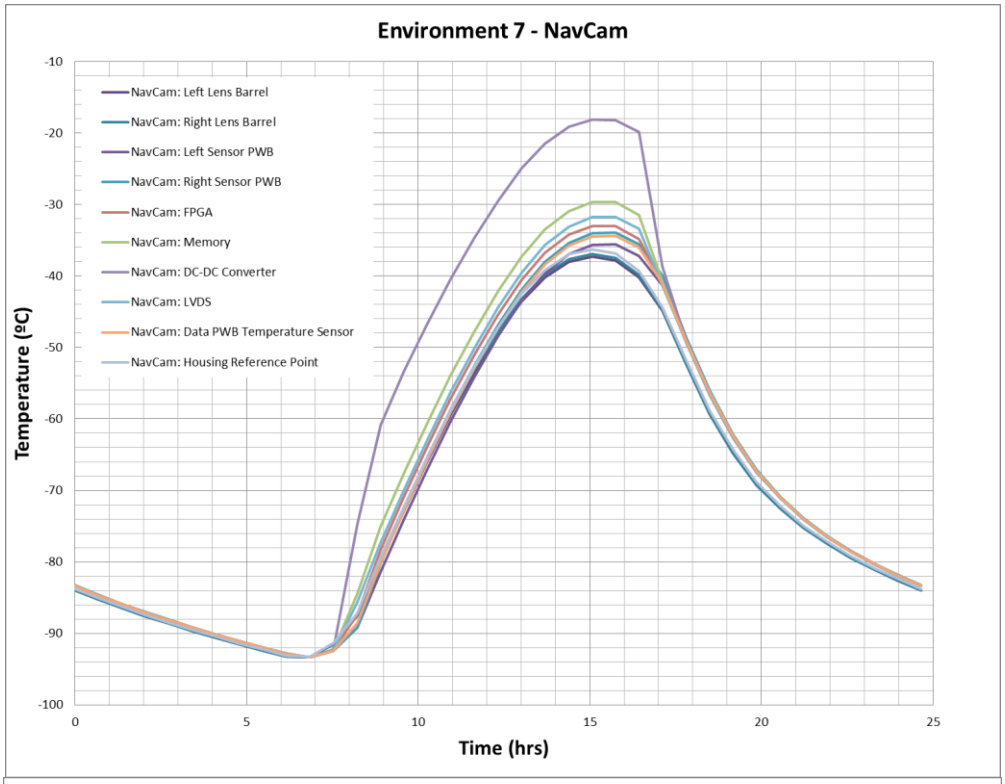

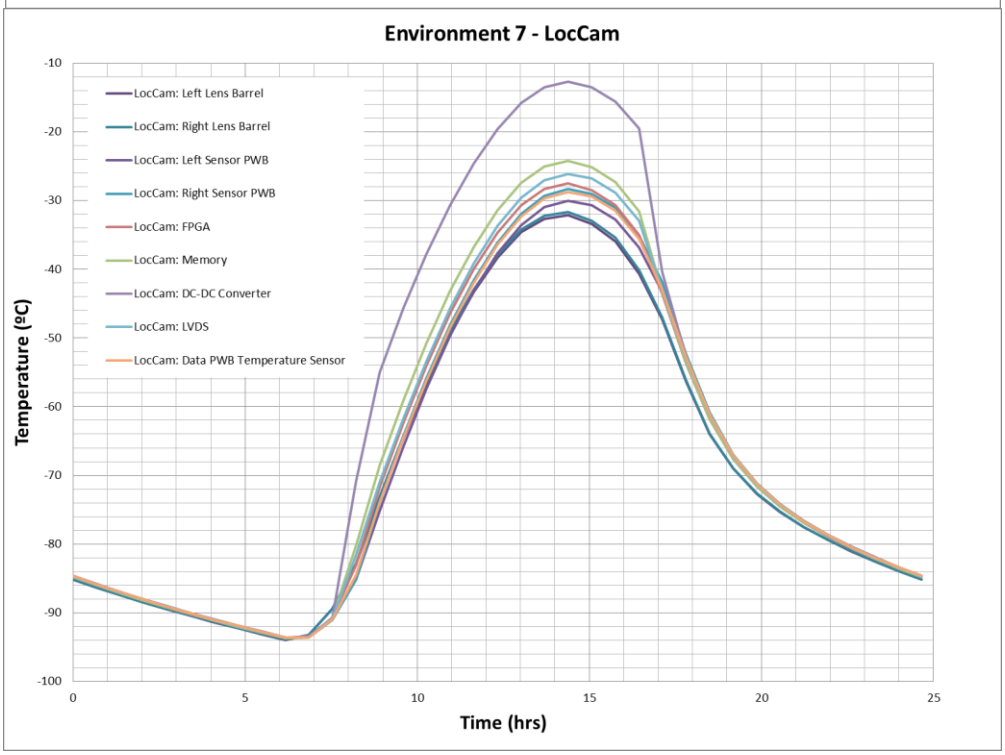

Figure 4 Temperature Profiles for Coldest Case

Table 4: Changes in Max. and Min.

Modified Mounting Conductance	Temperature Change			
	Hot		Cold	
	No Dust		Dust	
	Maximum Power		Minimum Power	
	Min	Max	Min	Max
NavCam FPGA	-4.60	6.84	-0.57	-2.06
NavCam LVDS	-4.57	6.82	-0.55	-6.20
NavCam DC-DC Converter	-4.56	6.47	-0.53	-1.52
NavCam Memory	-4.60	6.82	-0.56	-2.15
NavCam Left Lens Barrel	-4.55	6.50	-0.50	-1.53
NavCam Right Lens Barrel	-4.54	6.48	-0.49	-1.46
NavCam Left Sensor PWB	-4.59	6.84	-0.56	-2.04
NavCam Right Sensor PWB	-4.59	6.80	-0.55	-1.75
NavCam Power Wire	-4.58	6.57	-0.52	-1.48
NavCam Data PWB Temperature Sensor	-4.58	6.83	-0.55	-3.49
NavCam Housing Reference Point	-4.73	7.18	-0.61	-1.79
LocCam FPGA	0.11	1.01	0.07	-0.70
LocCam LVDS	0.12	0.98	0.05	-4.92
LocCam DC-DC Converter	0.12	0.95	0.07	-0.30
LocCam Memory	0.11	1.01	0.07	-0.82
LocCam Left Lens Barrel	0.10	0.79	0.07	-0.30
LocCam Right Lens Barrel	0.11	0.78	0.06	-0.25
LocCam Left Sensor PWB	0.11	0.97	0.07	-0.73
LocCam Right Sensor PWB	0.11	0.97	0.06	-0.46
LocCam Power Wire	0.11	0.94	0.07	-0.31
LocCam Data PWB Temperature Sensor	0.11	0.97	0.01	-2.20
LocCam Housing Reference Point	0.10	0.89	0.07	-0.22

The effect of dust is shown in Table 5.

The largest change is a temperature drop of 11.44 ºC for the NavCam right lens barrel. However, it should be noted that the NavCam housing reference point showed a temperature drop of 8.80 ºC which accounts for most of the temperature change. The actual change in camera thermal performance with the addition of dust is effectively a temperature drop 2.6 ºC. Table 6 shows the normalized temperature change, that is the temperature change with the change in TRP removed.

Table 5: Effect of Dust on Camera Temperatures

Effect of Dust	Temperature Change (ºC) Dust - No Dust			
	Hot		Cold	
	Typical Power		Typical Power	
	Min	Max	Min	Max
NavCam FPGA	-1.96	-9.55	2.10	4.22
NavCam LVDS	-2.02	-9.79	2.22	4.53
NavCam DC-DC Converter	-1.99	-9.30	2.26	4.40
NavCam Memory	-1.97	-9.57	2.10	4.25
NavCam Left Lens Barrel	-2.28	-11.36	1.84	4.83
NavCam Right Lens Barrel	-2.29	-11.44	1.88	4.44
NavCam Left Sensor PWB	-2.03	-9.76	2.17	4.34
NavCam Right Sensor PWB	-2.03	-9.74	2.19	4.32
NavCam Power Wire	-1.97	-9.41	2.30	4.50
NavCam Data PWB Temperature Sensor	-2.02	-9.77	2.20	4.51
NavCam Housing Reference Point	-1.76	-8.80	1.93	4.03
LocCam FPGA	-0.33	-4.38	-0.28	-2.01
LocCam LVDS	-0.36	-4.76	-0.31	-2.20
LocCam DC-DC Converter	-0.36	-4.62	-0.31	-2.05
LocCam Memory	-0.33	-4.40	-0.28	-2.02
LocCam Left Lens Barrel	-0.42	-6.02	-0.36	-2.73
LocCam Right Lens Barrel	-0.43	-6.13	-0.37	-2.75
LocCam Left Sensor PWB	-0.35	-4.62	-0.30	-2.06
LocCam Right Sensor PWB	-0.35	-4.69	-0.29	-2.10
LocCam Power Wire	-0.37	-4.66	-0.31	-2.07
LocCam Data PWB Temperature Sensor	-0.36	-4.72	-0.30	-2.19
LocCam Housing Reference Point	-0.27	-3.43	-0.23	-1.41

Table 6: Effect of Dust – Normalized to TRP Change

Effect of Dust	Normalized Temperature Change (ºC) Dust - No Dust			
	Hot		Cold	
	Typical Power		Typical Power	
	Min	Max	Min	Max
NavCam FPGA	-0.20	-0.75	0.17	0.19
NavCam LVDS	-0.26	-0.99	0.29	0.50
NavCam DC-DC Converter	-0.23	-0.50	0.33	0.37
NavCam Memory	-0.21	-0.77	0.17	0.22
NavCam Left Lens Barrel	-0.52	-2.56	-0.09	0.80
NavCam Right Lens Barrel	-0.53	-2.64	-0.05	0.41
NavCam Left Sensor PWB	-0.27	-0.96	0.24	0.31
NavCam Right Sensor PWB	-0.27	-0.94	0.26	0.29

NavCam Power Wire	-0.21	-0.61	0.37	0.47
NavCam Data PWB Temperature Sensor	-0.26	-0.97	0.27	0.48
NavCam Housing Reference Point	0.00	0.00	0.00	0.00
LocCam FPGA	-0.06	-0.95	-0.05	-0.60
LocCam LVDS	-0.09	-1.33	-0.08	-0.79
LocCam DC-DC Converter	-0.09	-1.19	-0.08	-0.64
LocCam Memory	-0.06	-0.97	-0.05	-0.61
LocCam Left Lens Barrel	-0.15	-2.59	-0.13	-1.32
LocCam Right Lens Barrel	-0.16	-2.70	-0.14	-1.34
LocCam Left Sensor PWB	-0.08	-1.19	-0.07	-0.65
LocCam Right Sensor PWB	-0.08	-1.26	-0.06	-0.69
LocCam Power Wire	-0.10	-1.23	-0.08	-0.66
LocCam Data PWB Temperature Sensor	-0.09	-1.29	-0.07	-0.78
LocCam Housing Reference Point	0.00	0.00	0.00	0.00

THERMAL DISTORTION CASES

The cases used for thermal distortion analysis were based on requirements supplied by the Neptec team and are listed in Table 7. The corresponding exterior temperatures are shown in Figure 5 and Figure 6.

Table 7: Cases Selected for TED analysis.

Case	Camera	Environment	Dust?	Power	Time (hr)	TRP Temp. (ºC)	Atmos. Temp. (ºC)
Hot	NavCam	1	No	Max.	15.75	42.6	-3.74
Cold	LocCam	5	No	Typ.	8.22	-62.2	-86.4

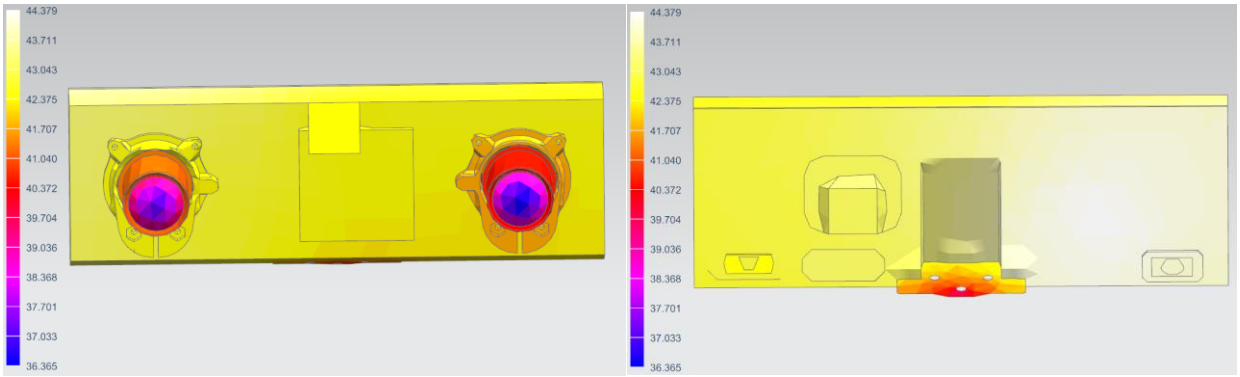

Figure 5: TED Hot Case Exterior Temperature Distributions (ºC)

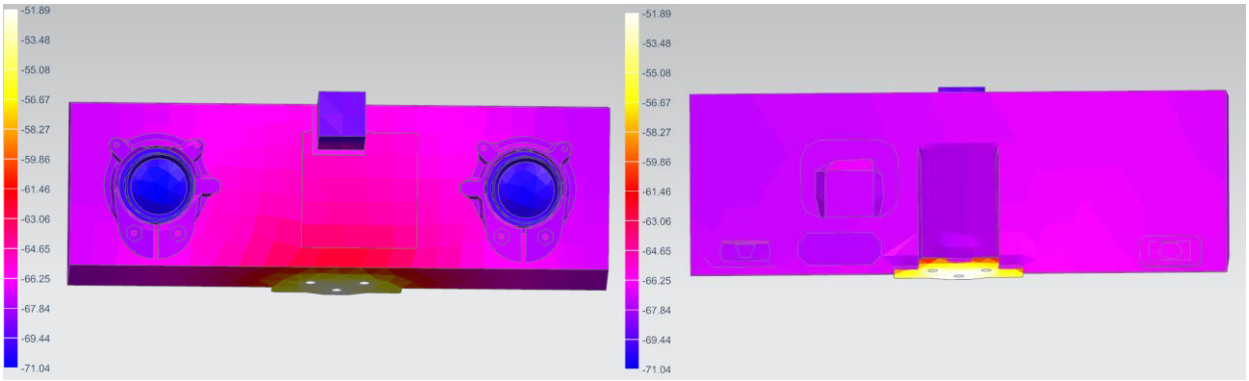

Figure 6: TED Cold Case Exterior Temperature Distributions (ºC)

TEMPERATURE MAPPING ONTO STRUCTURAL MODEL

Thermal and structural meshing requirements are fundamentally different. Having components meshed differently in terms of element type and level of details results in different node locations and quantity. This is why a temperature mapping process must take place to correctly transfer the calculated temperatures from the thermal model (source) onto the structural model (target).

This process starts by defining source mapping zones in thermal model and then associating them to target mapping zones in the structural model. Below is an illustration of how this process took place in Simcenter 3D:

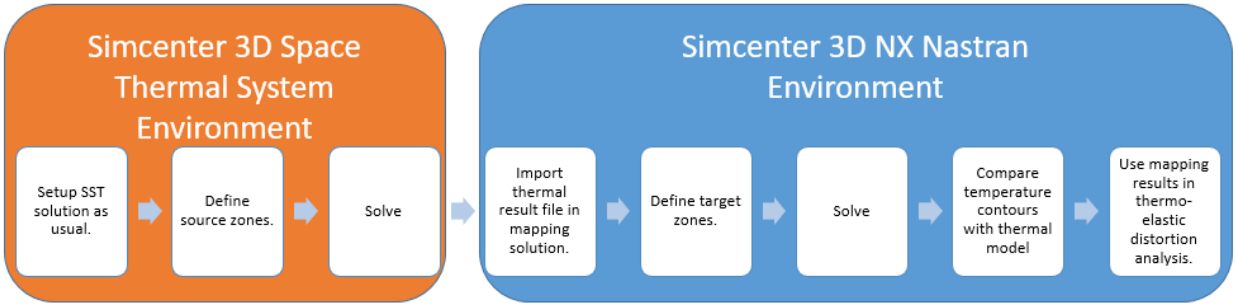

Figure 7: Temperature Mapping Process in SC3D

Two different types of mapping zones were used based on their representation in the thermal model. Parts represented with a single layer of shell elements or with solid elements used the

standard “Thermal Association Zone”. Parts represented with two layers of shell elements, i.e. PWBs, used a “Transverse Gradient Zone” in order to capture the temperature variation between the top and bottom surfaces. The “Transverse Gradient Zone” uses the two shell temperatures to calculate a mid-plane temperature and a through thickness gradient.

Source zones contain elements; target zones contain nodes. Each node in the structural model is associated with an element in the thermal model, based on zones and proximity and its temperature determined by interpolation within that element.

Figure 8 shows thermal and structural meshes of the lens assembly to give some indication of relative mesh densities.

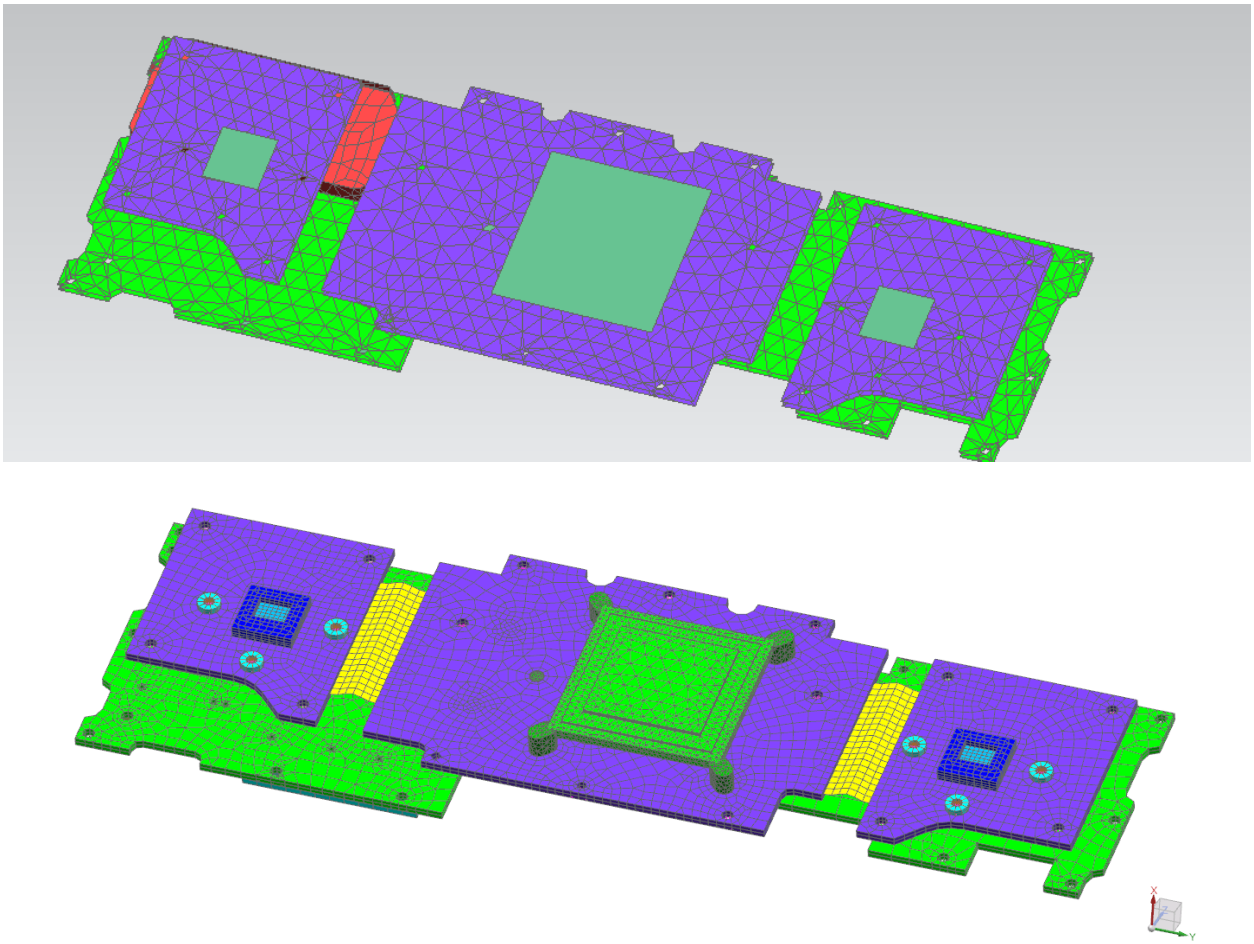

Figure 8 Thermal (top) and Structural Meshes of Electronics.

Figure 9 and Figure 10 show thermal vs mapped structural model temperature distribution for the hot thermal distortion case.

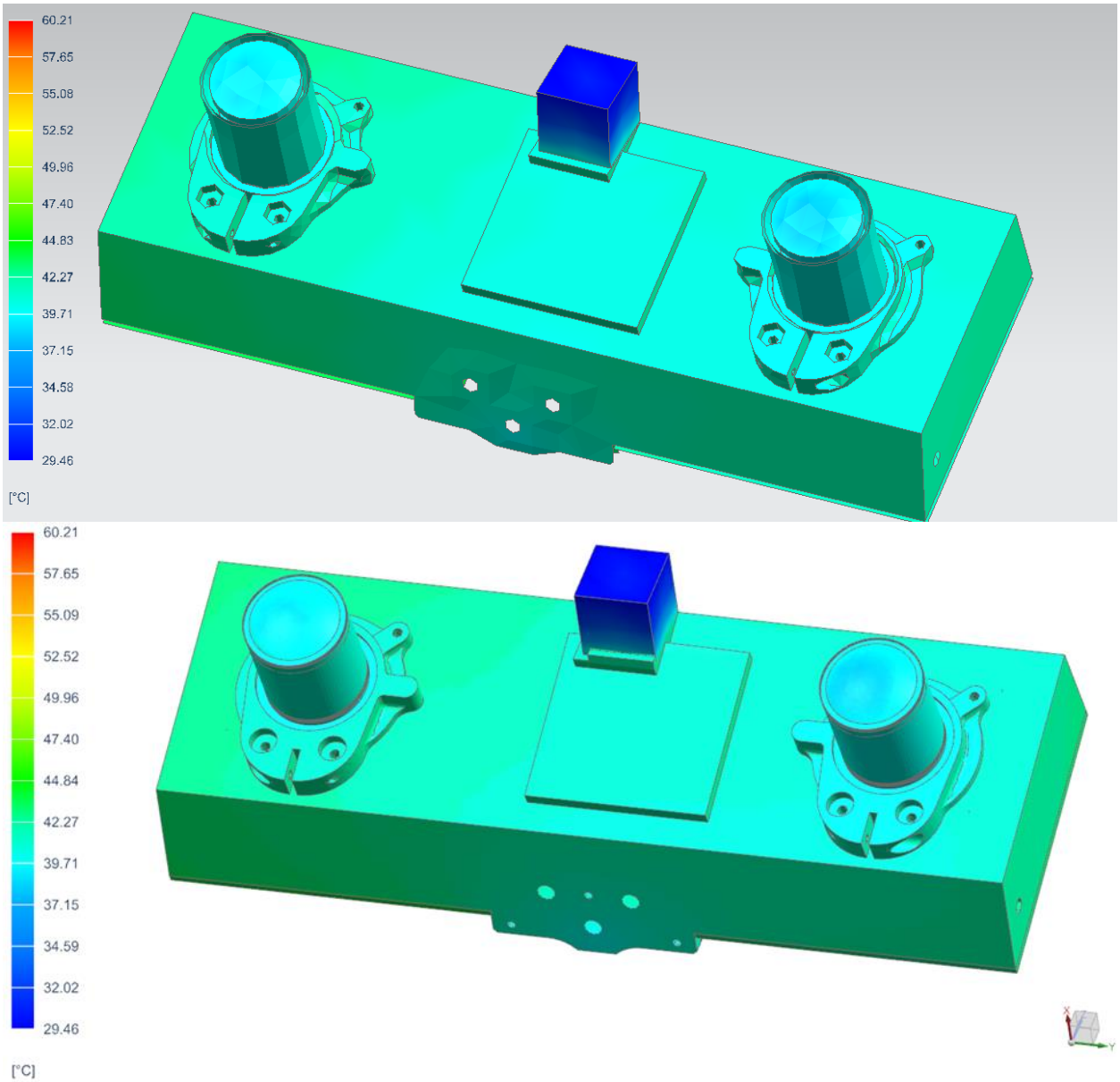

Figure 9 Exterior Temperatures for Thermal (top) and Structural Models

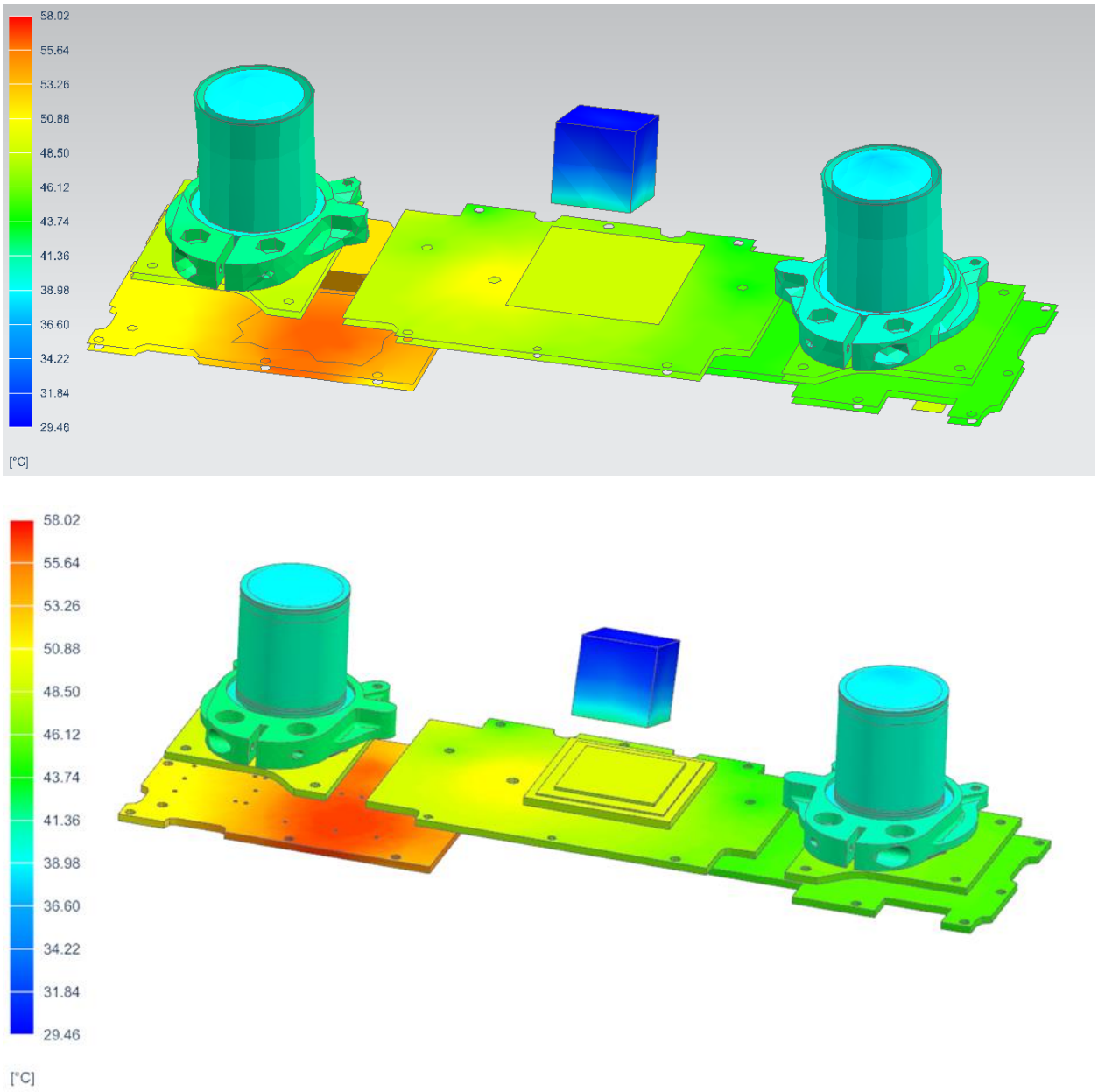

Figure 10 Interior Temperatures for Thermal (top) and Structural Models

THERMAL DISTORTION ANALYSIS

Using the temperature data mapped from the thermal model into the structural model a distortion analysis was used to quantify the linear and angular displacement of the optics and

the linear displacement of the detectors when in the hottest and coldest Martian environments.

From the previous analyses, the instant of the hottest and coldest Temperature Reference Point (TRP) was identified and the corresponding temperature distribution at the time when the extreme temperature occurred was used as the basis of the distortion analysis.

The hottest load case for distortion analysis was at the instant where the Temperature Reference Point (TRP) was hottest, i.e. closest to +50°C. Note that the resulting temperature of the TRP is lower than the maximum qualification temperature of +50°C.

Since we only care about thermal distortions while operating, the coldest for distortion analysis was defined as the instant where the Temperature Reference Point (TRP) was -60°C (coldest qualification temperature) and the air temperature was coldest. Since the temperature fell below -60°C at night for every load case examined, the second criteria of coldest air temperature was needed to select a single test case.

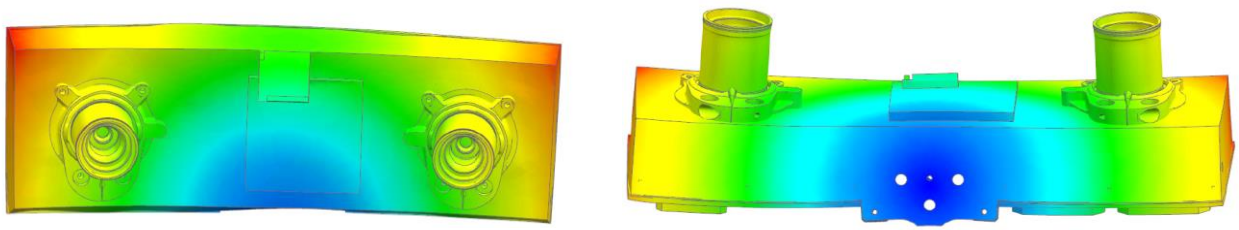

Figure 11 Exaggerated Thermo-elastic Distortions for the Hot Case

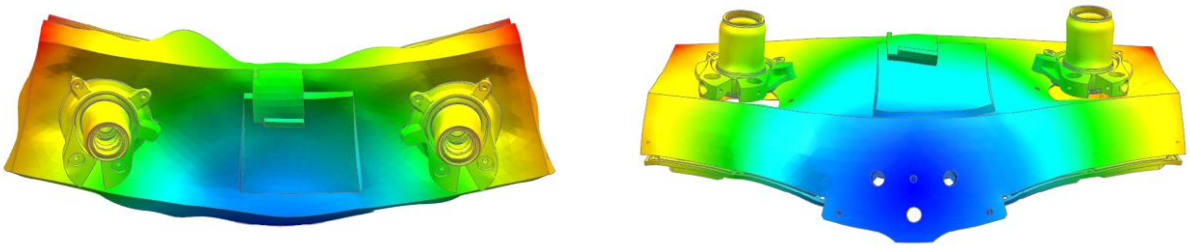

Figure 12 Exaggerated Thermo-elastic Distortions for the Cold Case

The intent of the thermal distortion analysis is to give an indication of the magnitude of change when at different temperatures. A full ray tracing of the displaced optics to find the new

optical center is beyond the scope of what was intended with this analysis. As such, a simplified approach was used to determine linear and angular changes in the optics.

The linear change in optical alignment was simplified and defined as the change in position of a point at the base of the optics located on the center of the bottom face of the filter element. The angular pointing direction of the optics was defined as the vector starting from the center of the bottom face of the filter element and going to the top face of the top lens. The position of the detector was determined from averaging the position of 3 points on the imaging plane. Angular changes in detector position are not evaluated, nor is change in focal length or optical distortion models. These effects were measured in test for each camera.

The results of the thermal distortion analyses are summarized in Table 8

Table 8. Thermal Distortion Results

Load Case	Temperature	Item	dX (μm)	dY (μm)	dZ (μm)	Total Linear (μm)	Total Angular (Arc Sec)
1	Coldest	Optics to Optics	1.10	-283.3	-0.901	283.3	11.6*
1	Coldest	Detector to Detector	1.09	-283.6	-1.27	283.6	n/a
2	Hottest	Optics to Optics	-0.554	76.2	-3.09	76.26	18.9*
2	Hottest	Detector to Detector	-0.2718	76.48	-3.38	76.56	n/a

**calculated based on best fitting plane at split clamp to front enclosure interface*

One may have expected the largest deformation to occur at cold because there is a greater temperature change from ambient when the unit is cold. However, Table 8 shows the largest distortion occurring when the camera is hot. This is because the camera dissipates 2.47 W when operating hot but only 1.81 W when cold during its operation. This is a difference of 36% more heat when operating hot. In addition, the coefficient of thermal expansion of the aluminum enclosure decreases as the unit is going cold. Both these effects lead to the hot case causing the greatest distortion.

The simplified pointing error effects are represented (graphically) by vectors as shown in Figure 13 and **Error! Reference source not found.**

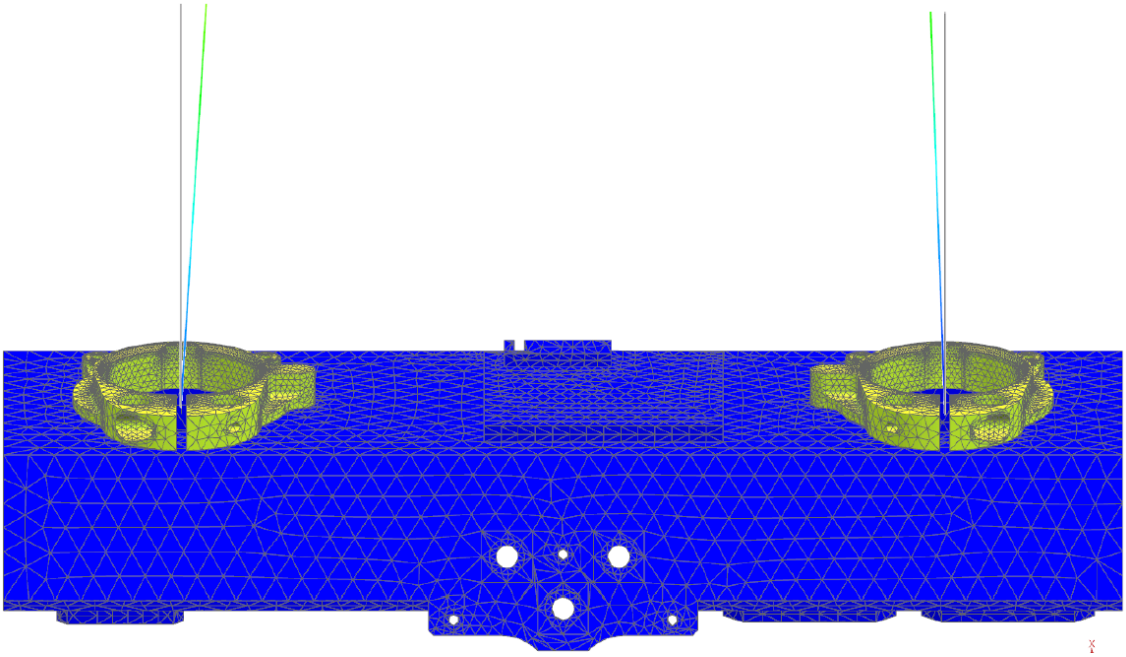

Figure 13 Simplified Lens Pointing Change for Hot Case

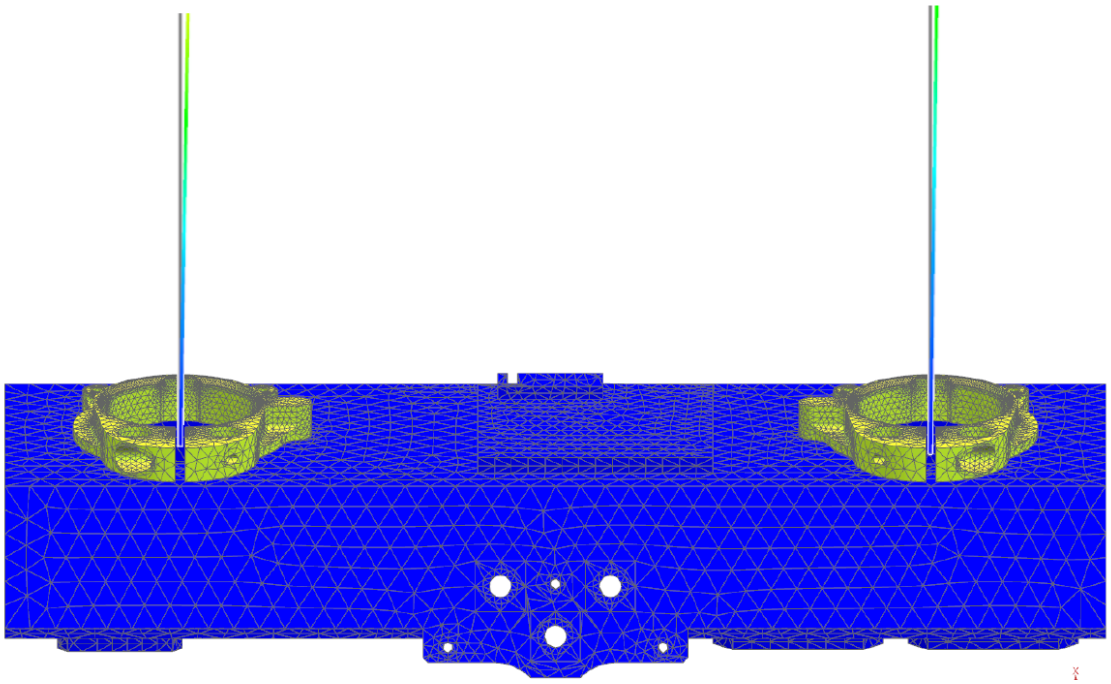

Figure 14 Simplified Lens Pointing Change for Cold Case

SUMMARY/CONCLUSION

A detailed thermal analysis of the ExoMars navigational and location cameras was performed to predict the temperature range experienced by each component in a number of different Martian environments. The hottest and coldest operational cases were then used to perform a thermo-elastic deformation analysis. Temperatures from the thermal model were mapped onto the NX Nastran structural model used to perform the thermos-elastic analysis.

The displacements from the thermo-elastic analysis were then used to determine relative displacement of lenses and sensor to evaluate impact on camera performance.